Radially resolved measurement of stator heat transfer in a rotor–stator disc system

D.A. Howey [a,*], A.S. Holmes [a], K.R. Pullen [b]

[a] Electrical Engineering Department, Imperial College, Exhibition Road, South Kensington, London SW7 2AZ, UK
[b] School of Engineering and Mathematical Sciences, Tait Building, City University, Northampton Square, London EC1V 0HB, UK

ARTICLE INFO

ABSTRACT

This paper describes a new experimental method for measuring stator heat transfer in a rotor–stator disc system using an electrical heater array. The system is partially blocked at the periphery, with radial outflow of rotor-pumped air from an inlet at stator centre. The aim is to improve thermal performance prediction for air-cooled disc type electrical machines. Local Nusselt numbers were measured for $0.6 < r/R < 1$ at three non-dimensional gap ratios $G = g/R = (0.0106, 0.0212, 0.0297)$ and rotational Reynolds numbers $3.7e4 \leqslant Re_\theta \leqslant 5.6e5$. Transition at the stator is observed to occur at $Re_\theta > 3e5$ for all gap ratios. Increased Nusselt numbers at the periphery are observed for all Re_θ and G because of the ingress of ambient air along the stator due to the rotor pumping effect.

© 2009 Elsevier Ltd. All rights reserved.

1. Introduction

Heat transfer in rotor–stator disc systems is important in many fields of engineering and especially crucial in disc type electrical machines and gas turbine engine internal air systems. Much attention has been focused on the latter but few studies have considered the former and there is significant scope for further work. Although disc type electrical machines such as the axial flux permanent magnet (AFPM) brushless machine have a long history, they have only been substantially researched since the advent of high performance rare-earth permanent magnet materials in the early 1980s. It is the *stator* heat transfer that is most relevant in these electrical machines, whereas the *rotor* heat transfer is usually of interest in turbomachinery, although stator heat transfer is still relevant. This paper therefore addresses the absence of suitable experimental data in this area, using a newly applied measurement technique.

Real electrical machines are geometrically more complex than the simplified rotor–stator system discussed here. However, studying a simpler system allows comparison with historical work on rotor–stator systems and provides a basic understanding of stator convective heat transfer.

2. Background and applications

In any electrical machine the stator temperature that will be reached at a given operating point must be predicted during design to ensure that the cooling provision is sufficient to avoid overheating. All electrical machines produce losses which manifest themselves in the production of heat, which raises the temperature of the materials within the machine, usually in the stator. The temperature that is reached in steady state is governed by the balance between heat input and heat removal. These materials, specifically permanent magnets and insulation polymers, can only withstand relatively low temperatures, typically 150 °C or less. Major sources of loss are Joule (I^2R) and core losses in the stator windings and Joule losses usually dominate in disc type machines. They increase with increased power drawn through the machine. Good electromagnetic design can be employed to minimise the losses for a given operating point but a rising heat input will always be apparent with increased power. On the other side of the equation, the rate of heat removal depends on the aerothermal design of the machine which is dependent on machine geometry, governing surface area for heat removal and heat transfer coefficient, which is governed by coolant fluid type and fluid dynamics. Another factor is the thermal capacity of the coolant: a fluid with low thermal capacity such as air may result in a bulk temperature rise that is too high. The power density is thus limited by the cooling provision and by material thermal limits. This is the situation for many electrical machines with the exception of certain cases in which the voltage regulation of the machine is so poor that the voltage across the load collapses before the thermal limit is reached.

For the reasons described, measurement and prediction of stator convective heat transfer coefficients is vital in the design of disc type electrical machines such as the machine shown in Fig. 1. At the stator surface, the local convective heat transfer coefficient h is a function of the fluid mechanics, i.e. the fluid properties,

* Corresponding author. Tel.: +44 (0) 20 7594 6215; fax: +44 (0) 20 7594 6308.
  E-mail addresses: d.howey@imperial.ac.uk (D.A. Howey), a.holmes@imperial.ac.uk (A.S. Holmes), keith.pullen.1@city.ac.uk (K.R. Pullen).

Nomenclature

Greek

ΔE	uncertainty in a measurement
ΔT	temperature difference (K)
ϵ	emissivity
μ	dynamic viscosity (kg/m s)
v	kinematic viscosity (m²/s)
Ω	rotational speed (rad/s)
ϕ	diameter (m)
ρ	density (kg/m³)
σ	Stefan–Boltzmann constant ($\sigma = 5.67e - 8$ Wm^{-2} K^{-4})

Roman

$\dot{m}$	mass flow rate (kg/s)
$\overline{Nu}$	average Nusselt number, ($\bar{h}R/k_{amb}$)
A	area (m²)
a/b	ratio of stator central opening radius to stator radius
b_x	constants ($x = 1,2,3,4$) used in heater calibration, see Section 4.3
C_m	moment coefficient ($T_q 0.5\rho\Omega^2 R^5$)
C_w	non-dimensional mass flow rate ($\dot{m}/\mu R$)
e	relative roughness (y/g)
F	view factor
G	gap ratio (g/R)
g	gap size (m)
h	convective heat transfer coefficient (W/m² K)
I	current (A)

k	thermal conductivity (W/m K)
Nu	local Nusselt number, (hR/k_{amb})
Q	heat flux, power (W)
q	specific heat flux (W/m²)
R	resistance (Ω), rotor outside radius (m)
r	local radial position (m)
Re_θ	rotational Reynolds number ($\Omega R^2/v$)
T	temperature (K)
T_q	torque on one side of rotor (Nm)
V	voltage (V)
y	absolute roughness height (m)
y^+	non-dimensional distance from wall (yv^*/v)

Subscripts

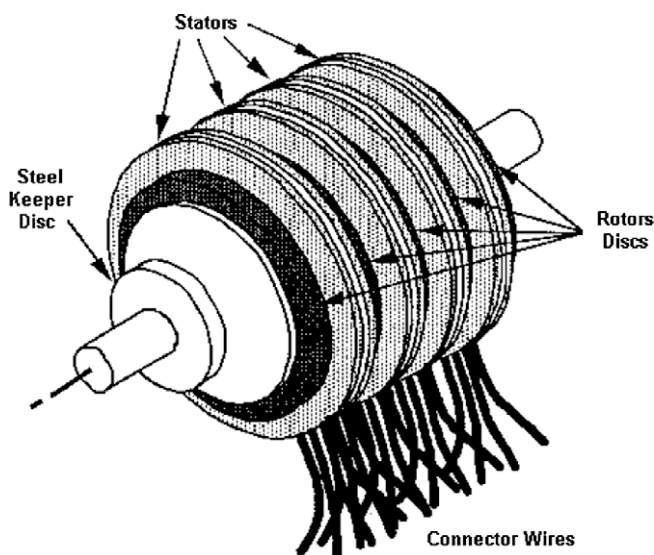|	
1	stator surface
2	rotor surface
amb	ambient
H	heater
Q	power
rad	radiative heat transfer
ref	reference (ambient)
s	stator
set	setpoint
TC1, TC2	thermocouple
V	voltage

Fig. 1. Air cooled multiple rotor high speed AFPM machine.

problem geometry and dynamics of the fluid motion past the surface. In forced convection the fluid motion is imposed by an external pressure difference rather than by density changes in the fluid; in the case of the disc type electrical machine the pressure difference is imposed by the rotation of the rotors. Air is typically introduced through holes in the rotor or by a hollow shaft.

A large body of theoretical, numerical and experimental work in the field of turbomachinery has been undertaken on rotor heat transfer in rotor–stator systems (see Section 3) and there is a good understanding of the fluid mechanics in the gap. However, there are very few published stator heat transfer results. The fluid velocity, pressure and temperature fields will not be axially symmetrical

and therefore the convective heat transfer coefficients at the stator are not the same as those at the rotor. Hence the rotor heat transfer results from existing research are not directly applicable and a new set of experiments (the subject of this paper) are being conducted in order to determine coefficients which are relevant in this application. The experimental objective is to measure the local and averaged stator Nusselt numbers $Nu = hR/k_{amb}$ and $\overline{Nu} = \bar{h}R/k_{amb}$ as a function of geometry, non-dimensional radial position r/R, rotational Reynolds number $Re_\theta = \Omega R^2/v$, gap ratio $G = g/R$ and non-dimensional air flow rate $C_w = \dot{m}/\mu R$.

3. Literature review

3.1. Rotor–stator heat transfer and disc type electrical machines

In 1921, von Kármán [1] derived steady state axisymmetric solutions of the Navier–Stokes equations for both laminar and turbulent flow over a single rotating free disc. These show that the disc drags fluid from the rotor centre to the outside edge and that fluid is drawn in axially towards the rotor to replace the fluid which has been pumped out. Dorfman [2] continued this work and examined analytical solutions and experimental results for laminar and turbulent flow and heat transfer for a rotating free disc. He also considered a rotor–stator system, discussing experimental results for the variation of moment coefficient $C_m = T_q/0.5\rho\Omega^2 R^5$ (T_q is the torque on one side of the disc) with rotational Reynolds number and gap ratio.

Rotor–stator systems exhibit more complex fluid mechanics compared to the free disc, and it is accepted [3] that, apart from a Couette-type flow that may occur for $G \leqslant 0.01$ at lower Reynolds numbers, there are generally two characteristic flow patterns. The first, Batchelor flow, is characterised by a rotating fluid core between two separate boundary layers, at the rotor and stator respectively. The boundary layers may be laminar or turbulent depending on G and Re_θ. The core rotational speed is approximately 40% of the rotor speed. Batchelor flow is usually observed in en-

closed rotor–stator systems where a recirculation of fluid from rotor to stator occurs at the outside edge. However, in rotor–stator systems which are open at the outside edge and also in systems with radial through-flow, the core rotation is diminished or destroyed. Instead, it is observed that the tangential velocity tends towards zero at the stator. This flow pattern is known as Stewartson flow.

Daily and Nece [4] measured moment coefficients in an enclosed rotor–stator system with no through-flow. They observed four distinct regimes depending on G and Re_θ: Regime I – merged laminar rotor and stator boundary layers, occurring for small values of G and Re_θ. Regime II – separate laminar boundary layers, at larger values of G and small Re_θ. Regime III – merged turbulent boundary layers at smaller G values and larger Re_θ. Regime IV – separate turbulent boundary layers at larger G and Re_θ values. Regimes II and IV correspond to a Batchelor type flow with core rotation. The distinction between each regime is not sharp but occurs over a range of values of G and Re_θ.

In both Batchelor and Stewartson patterns, the stator average convective heat transfer is likely to be less than that at the rotor because the fluid velocity gradients and therefore the wall shear stress at the stator will be lower than at the rotor. In a recent ESDU study [3] reviewing work on rotating discs, cylinders and cavities, there is a reference to torque measurements made on stationary discs with net radial inflow of air. It is noted that the measured stator torque was always lower than the rotor torque [3, p. 43].

In a disc type electrical machine a range of configurations are possible: the periphery may be fully enclosed, partially enclosed or open but surrounded by a grill or mesh. There may be significant rotor pumped radial through-flow and in high speed machines there may be fan or compressor assisted radial through-flow. It is therefore difficult to say definitely whether the flow will tend towards a Batchelor or Stewartson pattern since it depends on the particular configuration, and the actual flow pattern may be a combination of both regimes. In addition, many machines have magnets protruding from the rotor(s) and these will change the flow pattern. In the experimental rig discussed here, the periphery is partially blocked and there is radial through-flow which is pumped by the rotor.

There is little specific mention of stator heat transfer in the comprehensive book by Owen and Rogers [5] despite the discussion of a wide variety of rotor–stator configurations. However in an earlier paper by Owen, Haynes and Bayley [6], average stator Nusselt numbers were measured for different rates of coolant inflow at the stator centre in a rotor–stator system with radial outflow of coolant. For coolant flow rates $C_w > 20,000$ the authors found that the stator heat transfer became independent of Re_θ, but at $C_w = 0$, a dependence on Re_θ is observed although a limited number of data points are presented. Comparison with our results is given in Section 8.

Bunker et al. [7] measured both rotor and stator heat transfer in a rotor–stator system using a central jet of air impinging on the rotor. The authors heated the fluid prior to the jet and measured the fluid to stator and fluid to rotor heat transfer with a transient thermographic liquid crystal technique. Measurements were made at $0.025 \leqslant G \leqslant 0.15$ and $2e5 \leqslant Re_\theta \leqslant 5e5$. Many of the parameters used are close to the parameters presented here and therefore the results are compared in Section 8.

Yuan et al. [8] measured stator heat transfer in an open rotor–stator disc system with no radial inflow/outflow, using thermographic liquid crystals for stator temperature measurements. They compared results with a numerical simulation using the RNG $k - \epsilon$ turbulence model and a commercial CFD code, FLUENT. A limited range of gap ratios $G = (0.049, 0.073, 0.098)$ and rotational Reynolds numbers $1.42e5 \leqslant Re_\theta \leqslant 3.33e5$ were tested. Comparisons are made between our results and the results of Yuan et al. in Section 8.

Scowby et al. [9] attempted to measure pressure drop versus air mass flow rate at various speeds in an AFPM machine, and they also constructed an empirical one-dimensional model of convective heat flow through the machine. However, this approach presumes that there are no fluid recirculations, an assertion that is almost certainly incorrect particularly at the outside edge of the stator where there is likely to be fluid ingress. The authors comment in constructing their model that suitable stator convective heat transfer correlations could not be found.

Wang et al. [10] attempted to develop a one-dimensional thermofluid model for AFPM machines using a similar empirical approach to Scowby et al. The authors first derive a relationship between pressure drop and air mass flow rate at different rotational speeds, then construct a one-dimensional lumped parameter thermal network representing the air flow path through the machine – again, this implicitly assumes no fluid ingress at the periphery. The authors also apply rotor convective heat transfer coefficients from the literature to the stator because suitable stator heat transfer information is not available. The validity of the one-dimensional model is unclear from the experimental temperature measurements presented.

3.2. Measurement of convective heat transfer

Han et al. and Rohsenow et al. [11,12] review the available experimental techniques for convective heat transfer measurement which can be summarised as follows:

1. *Array of thin film heat flux gauges:* Comprising a differential temperature transducer separated by a thin thermal resistance of known properties. The heat flux through the surface to which each sensor is attached is determined by solving the conduction problem through the thin film. Uncertainties of typically 5–10% are achievable using commercially available sensors and instrumentation.

2. *Transient techniques:* These involve embedding a thermocouple array into a surface and then exposing the surface to a step-change in fluid temperature. By recording temperature transient response and assuming the convective heat transfer dominates over the conductive heat transfer at the surface, the heat transfer coefficients can be calculated.

3. *Infra-red (IR) thermography:* A uniform thermally insulating layer is applied to a heated block of conductive material such as aluminium. Surface temperatures are measured by an IR thermal imager and block temperatures by embedded temperature sensors. Heat flux is calculated by solving Laplace's equation for the surface insulating layer using the experimentally obtained boundary temperatures. The method is explained in Pellé, Boutarfa, Harmand [13–15]. Because of the insulating layer, the radial or tangential heat flux along the surface is small compared to axial heat flux through the surface. The method offers high spatial resolution and does not interfere with the flow, although for accurate results it requires in-situ calibration with known surface temperature reference points. Also, as Cooke [16] shows, solving for heat transfer by inverse analysis of temperature differences can produce very large uncertainties in certain scenarios.

4. *Thermochromic liquid crystals (TLCs) and thermographic phosphors:* TLCs reflect different colours of incident light depending on the local temperature. However, as discussed by Kowalewski et al. [17] they may have limited measurable temperature range (narrowband TLCs, eg. 4 K) or may be inaccurate (broadband TLCs). Because the technique is reflective, careful uniform illumination must be arranged. Thermographic phosphors are another technique where a phosphor coating on the surface is exposed to UV laser excitation and has a decay time which is

temperature dependent. This requires UV lasers and intricate experimental design with complex instrumentation to achieve the desired results.

5. *Array of thin-foil heaters:* Thin metal strips, typically stainless steel, are electrically heated to give a constant heat flux. Thermocouples beneath each strip measure the surface temperature and therefore the heat transfer coefficient can be calculated. A similar technique uses copper heaters to give regionally averaged measurements [12, section 6.2.4]. In contrast to the other techniques, thin-film heaters do not require a separate heating system.

The measurement technique presented in this paper is a variation on the thin-film heater technique. If constructed from a material such as copper, which has a positive temperature coefficient of resistance, thin-film heaters can also be used for temperature sensing. In the literature, this technique has been applied by Bae, Rule and Kim [18] to measure time and space-resolved heat transfer in a boiling process. The authors constructed a microscale heater array comprising 96 platinum heater elements deposited on a quartz substrate. The entire array measured 2.7 × 2.7 mm and each heater had a nominal resistance of 1000 Ω. The experiments also included a camera to correlate visual information with the heat transfer measurements. The heaters were each controlled by Wheatstone bridge circuits with op-amp feedback and a digital potentiometer allowing heater temperature control.

4. Design of experimental apparatus

4.1. Overview

A rotor–stator disc system, shown in Fig. 2, was constructed with the rotor driven at a set speed by a computer controlled servo motor. The experimental rig parameters are given in Table 1. The gap ratio was adjustable from $0.0085 \leqslant G \leqslant 0.0934$ by insertion of accurately machined spacers. The air exit gap at the periphery was not fully open but partially blocked, which is similar to the situation found in many generators. Air was pumped by the movement of the rotor from an inlet at the stator centre to four exits at the edge of the rotor–stator system. The air mass flow rate is derived from measurements of the gauge pressure at the air inlet pipe after a calibrated bellmouth entry.

The stator heaters, heat flux measurement and temperature sensing were combined into one device, a printed circuit board (PCB) with 14 concentric spiral shaped copper heater elements, each comprising a number of turns. Since the resistance of copper varies with temperature, the surface temperature can be mea-

Fig. 2. Cross section through experimental apparatus.

Table 1
Experimental rig parameters.

|		
Rotor diameter	471	mm
Rotor material	Aluminium	
Rotor thickness	16.5	mm
Maximum speed	3000	rpm
Clearance at outer edge	1.2	mm
Stator mount material	Tufnol	
Stator air inlet diameter	76.2	mm
Gap size g	2–22	mm
Gap ratio G	0.0085–0.0934	
PCB track width	550	μm
PCB inter-track gap	200	μm
Copper thickness	16	μm
Number of heaters	14	

sured. Each heater element consists of a number of concentric spirals, forming one long resistive copper track per heater. The pitch of the spirals is very slight and therefore although the heaters are spiral shaped they can be considered geometrically to be concentric annular rings. Two PCBs were produced: one with exposed tracks (PCB1), the other with a thin layer of epoxy (solder resist) bonded to the surface (PCB2) for a smoother finish. An accurately known voltage V is applied across each heater, resulting in a current $I = V/R$ flowing, depending on the heater resistance. The total heat flow from the heater can be calculated as $Q = IV$. The net convective heat flux is equal to $Q - Q_{rad} - Q_{cond}$ where Q_{rad} is the radiative heat transfer from stator to rotor and Q_{cond} is the conductive heat loss through the rear of the heater PCB. The values of Q_{rad} and Q_{cond} are small but not negligible; Q_{rad} is calculated directly and subtracted from Q, whereas Q_{cond} is included as a systematic uncertainty since it cannot be accurately known due to the lack of knowledge of thermal contact resistances between insulating layers in the experimental rig. The local convective heat transfer coefficient is given in Eq. (1):

$$h = \frac{IV - Q_{rad}}{A(T_s - T_{ref})} = \frac{q_{net}}{T_s - T_{ref}} \tag{1}$$

Strictly speaking, T_{ref} should refer to the local fluid bulk temperature at the radius where the measurement for h is being made. However, it is recognised [5] that it is often difficult to measure the local fluid bulk temperature. Therefore the accepted convention is to use the ambient inlet fluid temperature as the reference temperature and this convention is followed here.

Closed loop control of temperature is needed. This is accomplished by calibrating the heaters so that they can be used as resistance temperature sensors. In the case of copper the resistivity variation with temperature is found to be linear within the range of interest. During heat transfer measurements, a control system continually adjusts the voltage across each heater to maintain the required temperature. Each heater element was designed to have approximately the same resistance so that the control circuits could be identical. (The *exact* resistances were measured against temperature during the calibration process as described in Section 4.3.) Fig. 3 shows a section of the uncoated heater PCB1. Each individual copper track is 16 μm thick, 0.55 mm wide with 0.2 mm gaps between tracks; each heater comprises between 8 and 14 turns, chosen such that each has an approximate resistance of 30 Ω.

By using the control system to set every heater element to the same temperature, an isothermal surface is produced on each copper strip heater and heat transfer along the surface between adjacent heater elements can be assumed to be negligible. The use of the term 'local' with respect to heat transfer coefficients, heat flux, or temperature measurements in this paper refers to the averaged or 'lumped' measurements for each heater ring. Within each heater
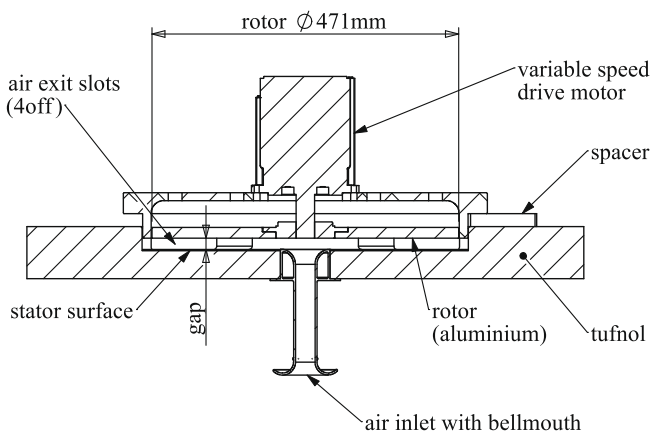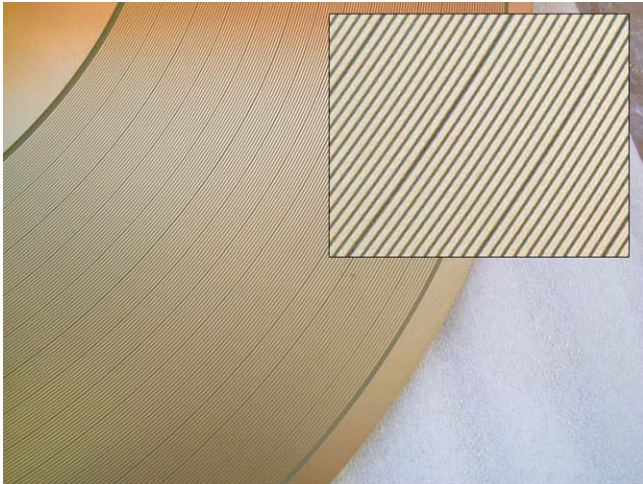
Fig. 3. Photograph showing uncoated heater PCB1 ($\phi = 0.5$ m).

element, variations in the r-direction and the θ-direction are therefore averaged. Variations between adjacent heaters, however, are resolved.

The rotor was machined from aluminium which is a thermally conductive material. This tends to produces an isothermal rather than an adiabatic rotor surface boundary condition in the experiment, with some heat transfer into the rotor expected. The rotor surface temperature was periodically measured during each experimental run by stopping the rotor and using a hand held surface temperature probe against the rotor surface. The convective heat transfer coefficients at the rotor–fluid interface are likely to be higher than those at the stator–fluid interface (as previously discussed) but the temperature difference between rotor surface and wall adjacent fluid is likely to be quite small, depending on the thickness of the stator thermal boundary layer.

4.2. Instrumentation and control

A block diagram of the heater control system for a single channel, which comprises two simple feedback control loops, is shown in Fig. 4. In total there are 14 identical channels – this number was chosen to give a balance between cost and spatial resolution.

The inner voltage control loop is constructed in hardware using high performance, low drift operational amplifiers with extremely low offsets (0.5 μV). A four-wire connection to each heater enables a differential amplifier to measure accurately the voltage drop across the heater, which is subtracted from a computer controlled reference voltage. The error signal is passed through an integrator circuit which drives a MOSFET. This inner loop compensates for any voltage drop in the heater power wires.

The outer temperature control loop is implemented in software. The actual heater temperature is calculated from the heater resistance, which is found by dividing the measured heater current into the voltage reference. A look up table containing calibration data is used for this purpose. A temperature PID controller responds to the temperature error, adjusting the reference voltage in order to bring the heater to the desired temperature T_{set}. The controller was tuned manually to give a reasonable response time whilst avoiding oscillation or excessive overshoot.

4.3. Calibration

All thermocouples apart from the surface temperature probe were calibrated in a water bath against a 5-point type J calibrated reference thermocouple supplied by Omega Engineering. They were found to have offset errors of less than 0.1 K apart from one thermocouple which had an offset error of 0.2 K. The thermocouple used for surface temperature measurements on the rotor could not be calibrated in this way, but being class 1, the uncertainty is reasonable (see Section 6).

The two heater PCBs were individually calibrated in a precision temperature controlled Lenton oven. Each was mounted horizontally to minimise the effect of temperature gradients. The heater, control circuits and DAQ system were calibrated together. The repeatability of results was measured by repeating the same test at two temperature setpoints on two separate days with the oven shut down overnight. It was found that temperature results were repeatable to within 0.1 K and current measurements were repeatable to within 0.1% based on two temperature setpoints and a range of applied voltages. The sensitivity to thermocouple repositioning was measured; it was found that at the same setpoint, temperature measurements in different positions differed by up to 0.2 K. Table 2 shows calibration data for PCB2 (for clarity the data for PCB1 are not included here). In this table, MSE is the mean square error for the linear fit; R^2 is the coefficient of determination, i.e. the proportion of variability in the data set that is accounted for by the statistical model; N is the number of data points lying outside a 95% confidence interval.

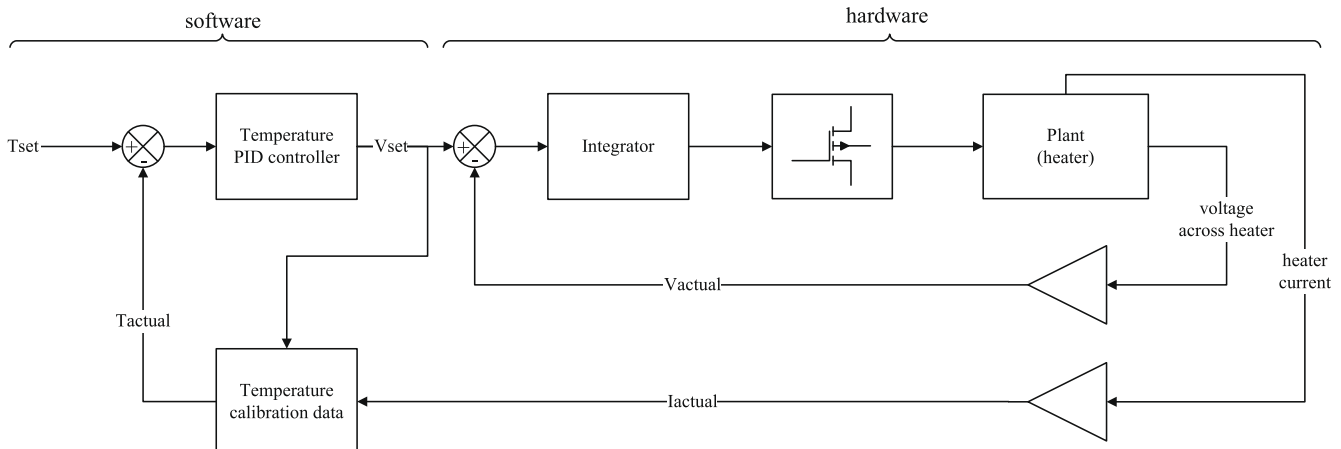For each heater, the resistance is given by Eq. (2), with T measured in C°:

Fig. 4. Block diagram of heater control system.

Table 2
Calibration data for coated heater PCB2.

Heater	1	2	3	4	5	6	7	8	9	10	11	12	13	14
b_1	26.416	26.461	25.93	27.422	26.386	25.175	23.499	27.284	25.481	26.517	27.3	28.243	26.033	26.445
$b_2 \times 10^{-2}$	1.8084	1.3068	1.2812	1.2434	1.1978	1.4897	1.6427	1.7533	1.0624	0.8747	1.018	1.0556	0.986	1.3068
$b_3 \times 10^{-1}$	1.1321	1.1368	1.1182	1.1877	1.1352	1.0863	1.014	1.1773	1.1056	1.149	1.1832	1.2194	1.1283	1.1376
$b_4 \times 10^{-5}$	−3.77	−3.96	−5.42	−8.41	−4.49	−4.47	−4.78	−5.99	−9.27	−9.16	−1.03	−7.16	−9.67	−5.22
MSE	0.0022	0.0012	0.0018	0.002	0.0012	0.0012	0.001	0.0019	0.002	0.0024	0.0018	0.0014	0.0018	0.0005
R^2	0.9994	0.9997	0.9995	0.9995	0.9997	0.9997	0.9997	0.9995	0.9994	0.9993	0.9995	0.9997	0.9995	0.9999
N	5	3	4	5	4	3	2	6	5	3	3	3	3	4

$$R = b_1 + b_2 V + b_3 T + b_4 (VT) \tag{2}$$

The term b_1 is the resistance at 0°C; b_2 is the coefficient of resistance with respect to applied voltage. This slight variation of the apparent measured resistance with voltage arises from offsets in the voltage and current measurement circuits. The coefficient of resistance with respect to temperature is given by b_3 and is about 0.1 Ω per K. Finally, b_4 is a cross correlation term accounting for any interaction between V and T, as can been seen this is virtually negligible. Rearranging Eq. (2) allows the heater temperature to be found from the voltage and current, Eq. (4):

$$T = \frac{R - (b_1 + b_2 V)}{b_3 + b_4 V} \tag{3}$$

$$\therefore T = \frac{\frac{V}{I} - (b_1 + b_2 V)}{b_3 + b_4 V} \tag{4}$$

4.4. Reduction of unwanted heat losses and heat gains

A number of unwanted heat loss and gain paths exist in the apparatus. The effect of these on the experimental results was quantified and minimised. The paths are as follows:

1. Conduction loss behind and around the circumference of the stator PCB.
2. Radiative heat transfer from stator to rotor.
3. Windage heating of the fluid due to viscous dissipation.

These items will now be addressed in turn:

Firstly, conduction heat loss behind the stator surface was minimised by mounting the PCB on 45 mm of Tufnol and 65 mm cork and polystyrene insulation. Using a simple one dimensional thermal conduction analysis it can be shown that the maximum heat loss is small, but not negligible. As already discussed, due to the lack of knowledge of the thermal contact resistances between insulating layers, the conduction heat loss has been accounted for as a systematic uncertainty, see Section 6.4.

Conduction heat loss in the radial direction at the innermost and outermost heated boundaries is unavoidable. In order to maintain the desired temperature, the inner and outermost heaters display a much greater apparent specific heat flux as a result of this edge effect. The heat flux at these heaters cannot be considered to represent the actual convective heat transfer and therefore only heaters 2–13 provide a reliable convective heat transfer measurement directly, see Section 5.2.

Secondly, the radiative heat transfer from the stator to the rotor depends on the temperature of each surface, the surface emissivities, and the view factor. An infra-red thermal imager[1] was used to measure the stator surface emissivity for the coated PCB2. This was accomplished by setting the stator to a known temperature, then calculating the emissivity along an isothermal line in the centre of the heated section in the image. This process was repeated 27 times

using different lines and difference focal lengths. The emissivity of the PCB2 was found to be 0.88 ± 0.10 (95% CI). The emissivity of PCB1 proved almost impossible to measure because the emissivity of the exposed conductors is very different to the emissivity of the gaps between the heaters. The emissivity of the conductors was found to be approximately 0.11, but this is not certain because low emissivities are difficult to measure due to reflections and directional effects. The FR4 substrate was found to have an emissivity of approximately 0.7. The average emissivity of PCB1 can therefore be taken as approximately 0.4.

The rotor, being polished aluminium, is estimated to have an emissivity of 0.05 or less [19].

The radiative view factor between two parallel coaxial discs depends on the gap size. A formula for calculating this is given by Incropera et al. [20, p. 817]; for small gap sizes $F_{12} \approx 0.95$. If the rotor and stator areas A_1 and A_2 can be assumed equal for the purpose of calculating radiative heat exchange, then the specific radiative heat transfer is given in Eq. (5):

$$q_{rad} = \frac{\sigma \left(T_1^4 - T_2^4 \right)}{\frac{1-\epsilon_1}{\epsilon_1} + \frac{1}{F_{12}} + \frac{1-\epsilon_2}{\epsilon_2}} \tag{5}$$

During experiments, the rotor temperature was periodically measured using a hand held temperature probe by stopping the rotor and applying the probe to the rotor surface. For each heat flux measurement, q_{rad} is calculated and subtracted from the total heater power to give the convective heat flux.
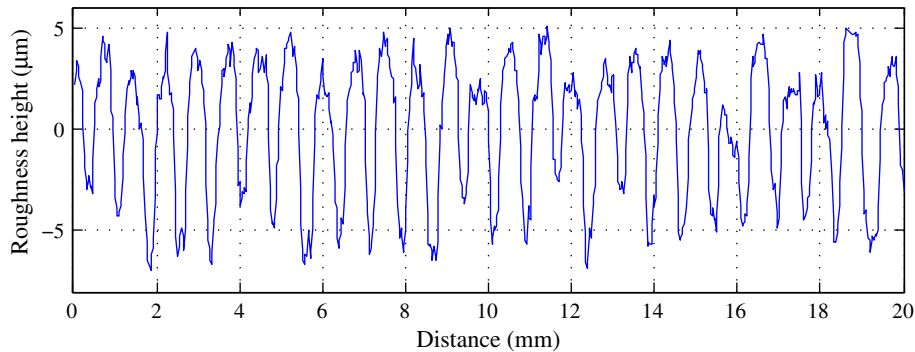
Finally, the importance of viscous dissipation can be quantified using the Eckert number, a non-dimensional group which is the ratio of kinetic energy to enthalpy, $Ec = U^2/c_p \Delta T$ where U is a characteristic flow velocity and ΔT is a characteristic temperature difference, typically 40 K for the system considered here, giving $c_p \Delta T \approx 40,000$. The highest velocities are found at the outer edge of the disc at high rotational speeds, for example $U = 74$ m/s at 3000 rpm, giving $U^2 = 5476$ m^2/s^2. Therefore it is estimated that in general, $Ec_{max} \approx 0.14$ although for the experimental results given here, the highest rotor speed was set at 1500 rpm giving $Ec_{max} \approx 0.03$. This is low enough that the effect of dissipation can be disregarded at this speed. Where future tests are operated at a maximum speed of 3000 rpm, the Eckert number is not negligible and viscous heating will lead to slightly increased bulk fluid temperatures. However, this increase mainly occurs near to the rotor, at the rotor tip, and it is suggested that the stator heat transfer is unlikely to be greatly affected. The situation is further complicated by another effect: fluid at ambient conditions tends to be entrained inwards at the stator at all but the smallest gap sizes. This will further decrease the likelihood that windage heating will affect the heat transfer measurements at the stator.

The viscous dissipation for the highest speeds presented here can be calculated from experimental correlations for moment coefficient which are presented in the literature. The most relevant for this geometry are those of Owen and Haynes [21], shown in Table 3, alongside correlations for the free disc as a reference case.

---

[1] FLIR Thermacam SC3000

Table 3
Rotor moment coefficient correlations.

Description	Correlation	Valid range	Reference
Laminar free disc	$C_m = 1.935 Re_\theta^{-0.5}$	$Re_\theta < 2e5$	ESDU [3, p. 21]
Turbulent free disc	$C_m = 0.073 Re_\theta^{-0.2}$	$5e5 < Re_\theta < 2e6$	Dorfman [2]
Rotor–stator with radial outflow	$C_m = \left(C_{m1}^6 + C_{m2}^6\right)^{\frac{1}{6}}$	$0 < Re_\theta \leqslant 4e10^6$	Owen & Haynes [21]
	$C_{m1} = 0.0553 \left(\frac{C_w}{G}\right)^{0.8} \frac{1}{Re_\theta}$	$\frac{g}{b} = 0.1333$	
	$C_{m2} = 0.0655 Re_\theta^{-0.186}$	$1.4e4 \leqslant C_w \leqslant 9.8e4$	
	$\times \left(1 + 12.4 \frac{C_w}{Re_\theta}\right)$	$0.01 \leqslant G \leqslant 0.18$	

Fig. 5. Measured surface roughness of PCB2.

From this it is possible to calculate the drag torque T_q, and therefore the windage heating $Q = T_q \Omega$ on one side of the disc, Eq. (6):

$$T_q = 0.5 C_m \rho \Omega^2 R^5 \qquad (6)$$

In the range of parameters of interest in this experiment, the equation for the turbulent free rotor gives a similar result to that for the rotor–stator with radial outflow, and the correlation of Owen and Haynes [21] is relatively insensitive to gap ratio, but is sensitive to Re_θ and C_w. For the maximum rotor speed tested the windage heating is calculated to be 5–10 W, which is about 3–5% of the applied heater power. At higher speeds, circulating air is allowed to cool the back of the rotor through holes in the rotor cover.

5. Performance

5.1. Surface roughness

In order to minimise the effect of rotor surface roughness on the heat transfer measurements, the rotor surface was polished during manufacture, to achieve a hydraulically smooth finish.

The roughness of the stator surface affects the convective heat transfer. It is generally accepted [3] that roughness does not affect the fluid shear stress in the turbulent flow regime if the absolute roughness height is less than the viscous sub-layer thickness, $y^+ < 5$. Daily and Nece [4] studied the effect of surface roughness on measured rotor moment coefficient and found that within the laminar regime, roughness has no effect. However, the onset of turbulence and the measured moment coefficients in the turbulent regime are affected by roughness, with rougher surfaces exhibiting higher moment coefficients (and therefore improved heat transfer compared to smooth surfaces).

In the present study, PCB1 has exposed tracks which are each 16 μm high so the maximum roughness height can be taken as this and the RMS roughness height as 8 μm. The surface roughness of PCB2 was measured using a surface profiler,[2] Fig. 5. The data have

_____
[2] Veeco Dektak

been corrected to remove low frequency skew because the sample was not perfectly flat. The RMS roughness of this data is 3.3 μm and therefore the maximum roughness height of PCB2 is ≈7 μm.

The relative roughness with respect to axial gap size can be calculated as $e = y/g$. For the smallest gap size examined here this gives a value of 6.4e−3 for PCB1 and a value of 2.8e−3 for PCB2. It is expected that PCB1 will exhibit higher average Nusselt numbers in the turbulent regime compared to PCB2, particularly at small gap ratios.

5.2. Stator temperature uniformity

The temperature uniformity of the heated stator under natural convection conditions (i.e. with the rotor disc and cover removed) was investigated using the thermal imaging camera. It was found that under these conditions the temperature of PCB2 heater was uniform to within ±0.7 K (95% CI) measured radially across the heaters. However, a boundary effect is observed at the inner and outermost heater radii, where a radial thermal gradient can be seen as shown in Figs. 6 and 7. This thermal gradient is due to the unavoidable radial heat flux at the heater boundary. The control system ensures that the average temperature of the inner and outermost heaters is held at the temperature setpoint, but a small temperature gradient develops across each. In Fig. 7, the average temperature of heater 1 is 327.7 K (54.6 °C), and that of heater 2 is 328.1 K (55 °C), which demonstrates that the control system is functioning correctly with $T_{set} = 55$ °C. Looking at the temperature gradient, heater 1 has to sustain a significant radial heat flux out of the boundary. There is also a small radial heat flux from heater 1 into heater 2. This has an almost negligible effect on the results, but it can be removed by marginally lowering the temperature setpoint for the boundary heaters.

The temperature uniformity of PCB1 was difficult to determine using infra-red imaging because of the huge difference in emissivity of the exposed gold-plated copper tracks in comparison to the substrate. However, the gaps between tracks are small (0.2 mm) and the temperature drop to the mid-gap point is likely to be

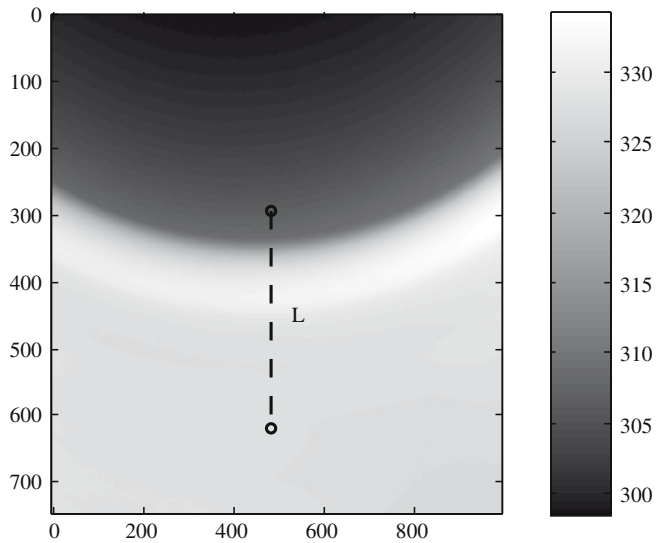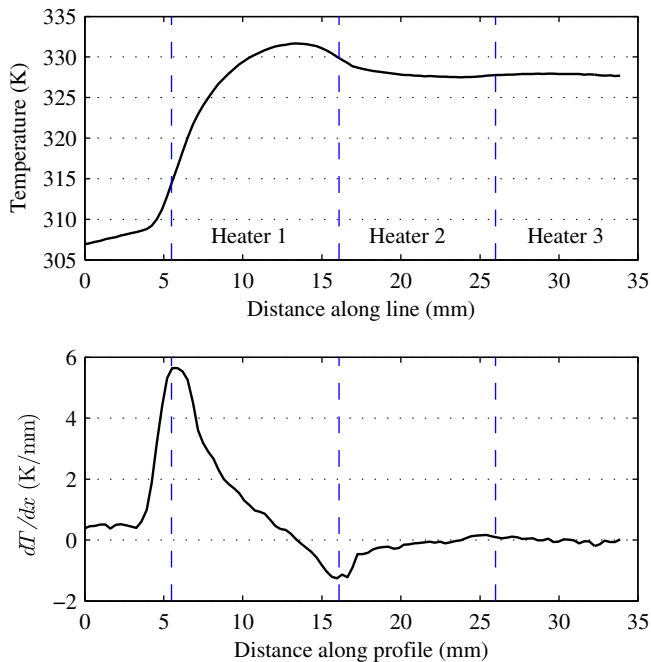**Fig. 6.** Heater edge temperature (K) at $T_{set} = 55°C$.

Fig. 7. T and dT/dx along line L (Fig. 6).

insubstantial, hence the thermal boundary condition for PCB1 should be close to uniform in temperature.

6. Uncertainty analysis

6.1. Thermocouples

Thermocouples apart from the surface probe were calibrated as described in Section 4.3. Combining the uncertainties, the total uncertainty in thermocouple temperature measurements is calculated to be $\Delta E_{TC1} = 1.44$ K. A class 1 type E thermocouple probe was used for rotor surface temperature measurements and this could not be calibrated at the same time as the other thermocouples. The total uncertainty for this thermocouple is calculated to be $\Delta E_{TC2} = 1.56$ K. Uncertainty margins are given for a 95% confidence interval (CI).

6.2. Heater voltage, current and power

The accuracy of resistors used in the control circuits was 0.1% and the current sense resistor had an accuracy of 1%. Therefore the uncertainty in the current measurement is calculated to be $\approx 1\%$, ignoring uncertainties in the op-amp itself, which should be negligible for this type of op-amp at steady state. The uncertainty in the data acquisition system is far smaller than this, of the order of 0.01% and therefore can be disregarded.

The uncertainty in the voltage feedback circuits was measured directly by applying a set voltage of 5 V, 10 V or 20 V across the heaters and measuring the actual voltage across each heater using a digital multimeter. It was found that the uncertainty in voltage measurements is $\Delta E_V = \pm 30$ mV (95% CI).

The uncertainty in power measurements depends on the applied voltage, but following the above discussion it can be seen that the uncertainty in current measurement dominates and therefore the uncertainty in power measurements is likely to be around 1%. More specifically, since $Q = IV$, the uncertainty in power is given by Eq. (7):

$$\Delta E_Q = \sqrt{\left(\frac{\partial Q}{\partial I}\Delta E_I\right)^2 + \left(\frac{\partial Q}{\partial V}\Delta E_V\right)^2} = \sqrt{(V\Delta E_I)^2 + (I\Delta E_V)^2} \tag{7}$$

For example, if the voltage applied is 30 V and the current drawn is 1 A, then the power is 30 W and the uncertainty is given by $\Delta E_Q = \sqrt{(30 \times 0.0102)^2 + (1 \times 0.03)^2} = 0.31W$ which is $\approx 1\%$ as expected.

6.3. Heater temperature

Measured heater resistances were calibrated against temperature and applied voltage as discussed in Section 4.3, removing systematic errors in heater temperature measurements caused by the circuits, but leaving systematic uncertainties caused by the reference thermocouple and calibration oven. The various uncertainties in the calibration process are as follows: calibrated reference thermocouple, $\pm 0.22 K$; DAQ system, $\pm 1.4 K$; oven temperature uniformity, $\pm 0.2 K$; oven temperature stability and repeatability, $\pm 0.1 K$. Combining these gives $\Delta E_H = \pm 1.44 K$.

6.4. Conductive heat loss

The conductive heat loss through the rear of the experiment introduces a small bias to the results but due to the lack of accurate knowledge of the thermal contact resistances between adjacent insulating layers, this must be included as a (one-sided) uncertainty $\Delta E_{Q_{cond}}$ rather than directly subtracted from the measured heat flow. The worst case conductive heat loss occurs when the stator surface convective heat transfer is smallest, whence the conductive loss will be a larger proportion of the measured heater power. It can be shown for the experimental results presented in this paper in general that $0.014Q < \Delta E_{Q_{cond-MAX}} < 0.07Q$.

6.5. Radiative heat loss

The radiative heat exchange between stator and rotor is calculated using Eq. (5) and for a typical experimental run the figure is reasonably constant since the rotor and stator surface temperatures do not change substantially. For example, typically $T_S = 333$ K and $T_R = 300$ K and therefore $q_{rad} \approx 11$ W/m^2, which is a small but not negligible fraction of the heater power. This figure itself is subject to some uncertainty since the temperatures and emissivities are subject to uncertainties. An analysis of the partial derivatives of Eq. (5) shows that typically $\Delta E_{Q_{rad}} \approx 4.7$ W/m^2 for

PCB1 and $\Delta E_{Q_{rad}} \approx 4.2\ W/m^2$ for PCB2 under the aforementioned conditions.

6.6. Convective heat transfer coefficient

The convective heat transfer coefficient was defined in Eq. (1). If the uncertainty in A can be ignored (a reasonable assumption given the accuracy of the manufacturing process), then the uncertainty in h can be derived by calculating the partial derivatives of h with respect to q, q_{rad}, T and T_{ref}. This is given by Eq. (8) (since the uncertainties in T and T_{ref} are essentially the same they have been grouped into one term):

$$\Delta E_h = \sqrt{\frac{\Delta E_{q_{net}}}{\left(T - T_{ref}\right)^2} + 2\,\frac{q_{net}^2}{\left(T - T_{ref}\right)^4}\left(\Delta E_T\right)^2} \qquad (8)$$

In this equation, in the case of $+\Delta E_h$, the term $\Delta E_{q_{net}}$ is equal to $(\Delta E_q)^2 + (\Delta E_{q_{rad}})^2$ but in the case of $-\Delta E_h$, $\Delta E_{q_{net}} = (\Delta E_q)^2 + (\Delta E_{q_{rad}})^2 + (\Delta E_{q_{cond}})^2$ due to the inclusion of the uncertainty caused by conduction (Section 6.4).

For example, if $q = 1000\ W/m^2$, $T = 333\ K$ and $T_{ref} = 293\ K$ and uncertainties are as per the previous sections then $h = 24.7 \pm 1.29\ W/m^2\ K$ (95% CI), which is an uncertainty of around 5% and is dominated by the uncertainties in the temperature measurements.

7. Results

A set of measurements was made using the uncoated PCB1 and rotor speeds from 100 to 1500 rpm with three gap sizes (2.5 mm, 5 mm, 7 mm). This is equivalent to a range of rotational Reynolds numbers of $3.7e4 \leqslant Re_\theta \leqslant 5.6e5$ and gap ratios $G = (0.0106, 0.0212, 0.0297)$. Fig. 8 shows the average stator Nusselt number results for all three gap sizes and for comparison also shows Nusselt number correlations after Dorfman [2] and Owen et al. [6] for a free rotor in the laminar and turbulent regimes. Figs. 9–11 show the local radially resolved results for each separate gap ratio respectively. Note that the average Nusselt numbers are not calculated across the entire stator, but from $r/R = 0.6$ to $r/R = 1$ since this was the area that was heated and this is the area most relevant to disc type electrical machines.
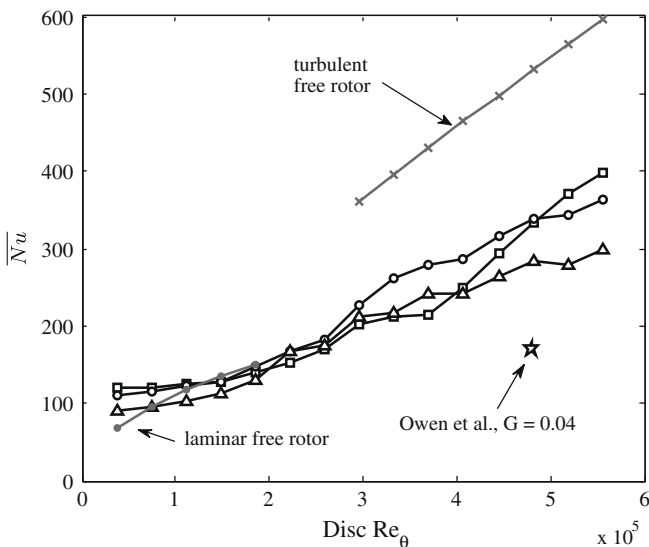

Fig. 9. Nu vs. r/R, $G = 0.0106$, $Re_\theta = 3.7e4(\times)$, $1.9e5\ (\bullet)$, $2.6e5\ (+)$, $3.3e5\ (\diamond)$, $4.1e5\ (\triangle)$, $4.8e5\ (\square)$, $5.6e5\ (\bigcirc)$.

8. Discussion

8.1. The effect of flow features on stator heat transfer

Referring first to the local radially resolved heat transfer results for the three gap ratios presented (Figs. 9–11), a number of interesting features of the fluid flow can be observed. At the smallest gap size $G = 0.0106$ that was measured (Fig. 9), a local increase in Nusselt numbers is observed at the outer radii. For example at $r/R > 0.9$ and $Re_\theta < 2.6e5$, Nu increases from approximately 100 to more than 200. As Re_θ is further increased, this effect becomes more pronounced and moves further inward along the stator. It is suggested that the increased Nusselt numbers at outer radii are caused primarily by ingress of cold (ambient temperature) fluid at the stator, which is one of the most important features of stator heat transfer in the rotor–stator system at the radii of interest in disc type electrical machines. The drop in bulk mean fluid temperature caused by the inflow increases the stator convective heat

Fig. 8. $\overline{Nu}$ vs. Re_θ for three gap ratios $G = 0.0106$ ($\square$), $G = 0.0212$ ($\bigcirc$), $G = 0.0297$ ($\triangle$), free disc ($\bullet$,$\times$) and stator result of Owen et al. ($\star$) also shown [2,6].
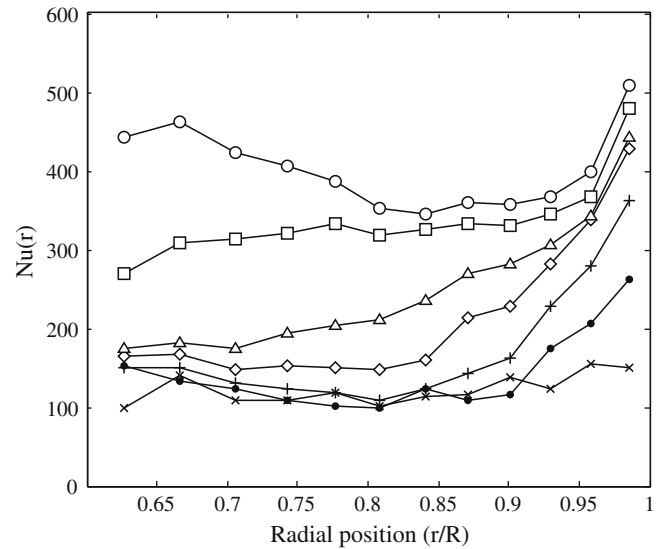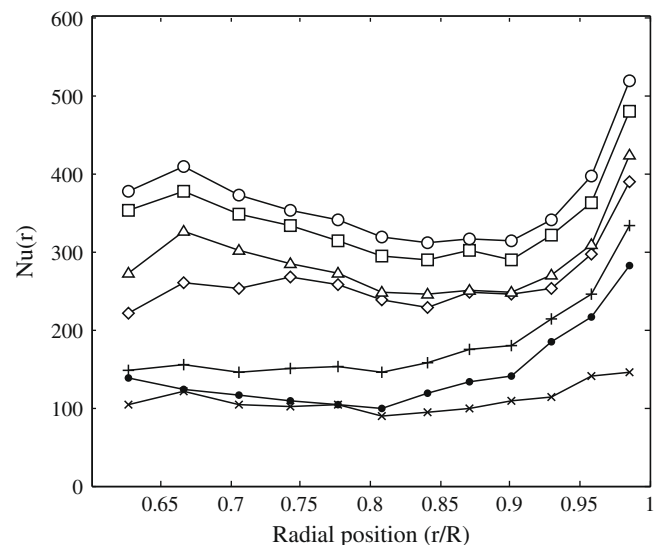

Fig. 10. Nu vs. r/R, $G = 0.0212$, $Re_\theta = 3.7e4\ (\times)$, $1.9e5\ (\bullet)$, $2.6e5\ (+)$, $3.3e5\ (\diamond)$, $4.1e5\ (\triangle)$, $4.8e5\ (\square)$, $5.6e5\ (\bigcirc)$.

Fig. 11. Nu vs. r/R, G=0.0297, $Re_\theta = 3.7e4$ ($\times$), $1.9e5$ ($\bullet$), $2.6e5$ ($+$), $3.3e5$ ($\diamond$), $4.1e5$ ($\triangle$), $4.8e5$ ($\square$), $5.6e5$ ($\circ$).

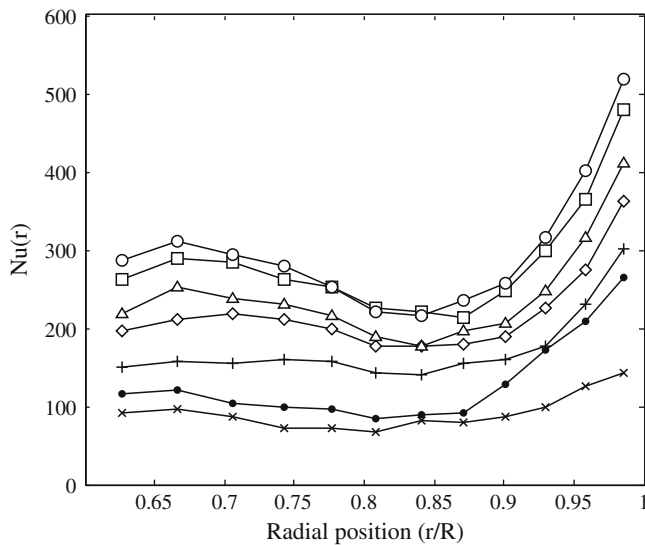transfer rate. This increases the presented values of Nu since the ambient air temperature was used as the reference temperature in defining Nu. As the gap ratio G is increased, the ingress of cold fluid at the outer edge becomes slightly more pronounced, this can be seen in Figs. 10 and 11 where $Nu > 500$ at $r/R > 0.9$.

Owen et al. [6] note that the peripheral inflow increases with increasing G and Re_θ, affecting the stator surface conditions far more than the rotor surface conditions. The effect can clearly be seen in the PIV results presented by Boutarfa et al. [13]. The reason for the inflow is that in the rotor–stator system the rotor boundary layer becomes thinner with increasing radius. As r increases, the air near the rotor is accelerated but also must pass through an increasingly large cross sectional area $A = 2\pi r\delta$ where δ is the rotor boundary layer thickness in the axial direction. Since the fluid density does not change significantly, δ must decrease as r increases according to conservation of mass. The tendency is for air near the stator to begin moving radially inwards where the rotor boundary layer is thinnest (at the outer periphery), causing an inbound secondary flow along the stator which feeds additional fluid into the rotor boundary layer. The penetration distance of this inbound flow depends on G and Re_θ and it is present to some extent even at the smallest values of G, as can be seen. In turbomachinery, hot gases are present at the disc periphery and such an air ingress is therefore to be avoided, by two means: the fitting of a shroud to the rotor or stator, and by forced pumping of coolant into the gap to thicken the rotor boundary layer at the periphery. In electrical machines however, the ingress may be advantageous in improving stator cooling.

The second flow feature that can be observed is the onset of transition from laminar to turbulent flow. The heat transfer remains approximately steady in the laminar regime at $Nu(r) \approx 100$ for $Re_\theta < 3.3e5$ at $r/R < 0.9$, but the values of Nu at $r/R < 0.85$ increase markedly for $Re_\theta > 3.3e5$, from approximately 150 to more than 400. Transition is less marked at the larger gap ratios but nonetheless begins also at $Re_\theta \approx 3e5$. It is unclear whether transition is complete and the stator boundary layer has become fully turbulent by $Re_\theta = 5.6e5$. Further data are required at $Re_\theta > 5e5$ in order to draw conclusions about the fully turbulent regime. A comparison with the free disc is informative: It is recognised [3, section 4.2] that transition on a free rotor typically begins to occur at $Re_\theta \approx 2e5$ and the flow is completely turbulent by $Re_\theta \approx 3e5$.

A small decrease in local Nusselt numbers between $0.65 < r/R < 0.9$ is seen at the higher Reynolds numbers for all gap ratios and this is more prevalent at the larger gap ratios. This is caused by local bulk fluid temperature increasing with radius due to the stator heating and is another consequence of using ambient air temperature rather than local bulk fluid temperature as the reference temperature in the definition of the Nusselt number.

Referring to the average stator heat transfer results (Fig. 8), it can be seen that in the laminar regime, stator average Nusselt numbers are very similar to the laminar flow average Nusselt numbers for an isothermal free rotor given by Dorfman [2] (valid for $Re_\theta < 1.8e5$), shown in Fig. 8 and given by Eq. (9):

$$\overline{Nu}_{lam} = 0.35Re_\theta^{0.5} \tag{9}$$

The correlation for turbulent regime average Nusselt numbers (valid for $Re_\theta > 2.8e5$) for an isothermal free rotor is given by Owen, Haynes and Bayley [6], Eq. (10):

$$\overline{Nu}_{turb} = 0.0151Re_\theta^{0.8} \tag{10}$$

This correlation is also shown in Fig. 8 and it can be seen that the measured stator heat transfer is considerably less than the free disc turbulent rotor heat transfer at the equivalent value of Re_θ.

8.2. Comparison to the results of others

To verify the measurement method used for heat transfer, a comparison can be made between the local Nusselt number results presented here and the results of Bunker et al. [7] and Yuan et al. [8]. Bunker et al. give locally measured Nusselt numbers for $G = 0.05$ for various Re_θ and $r/R < 0.9$ using a technique reported to have a measurement uncertainty of 10%. Fig. 12 shows the results in comparison to those presented here. As can be seen, measured values of Nu are close particularly at $Re_\theta = 5e5$ and $Re_\theta = 3.5e5$. The results at $Re_\theta = 2e5$ however are different; this difference may have been caused by a combination of factors including the presence of a peripheral shroud and the greater gap ratio in Bunker et al.'s experiment, which are not present in the experimental rig presented here.

Yuan et al. give results also at $G = 0.05$ and $r/R < 0.85$ for a rotor–stator system with no central admission of air at the stator. These are shown in Fig. 13 for comparison. Trends are similar but the local results are very different to those measured here. It is sug-
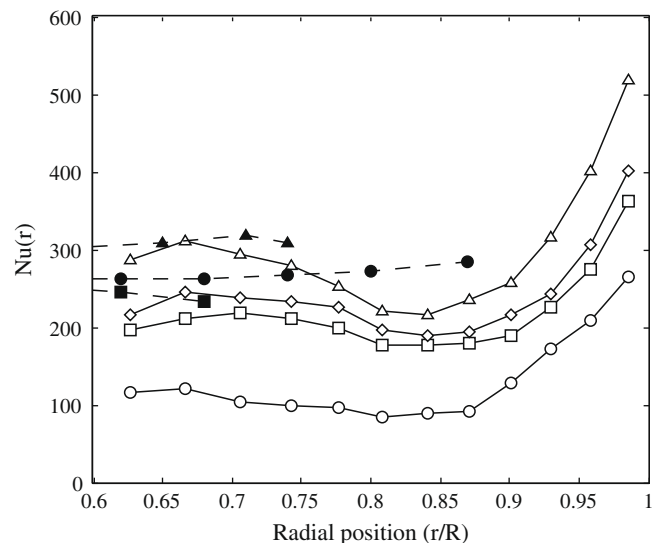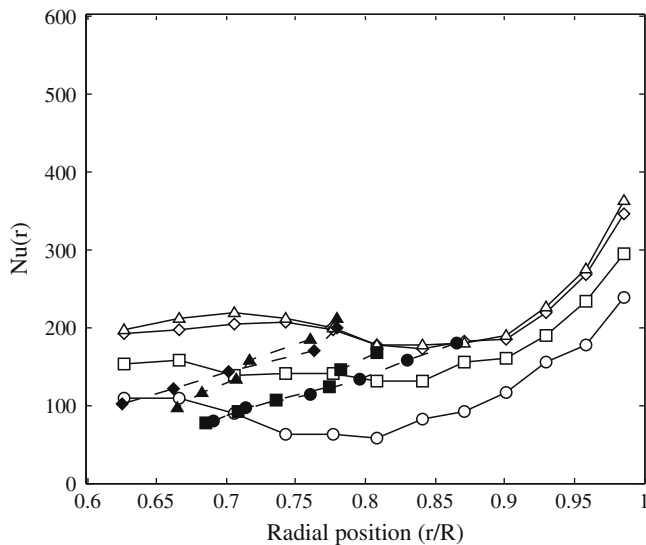

Fig. 12. Comparison between G=0.0297 at $Re_\theta = 1.9e5$ ($\circ$), $3.3e5$ ($\square$), $3.7e5$ ($\diamond$), $5.6e5$ ($\triangle$), vs. Bunker et al. [7] at $G = 0.05$ and $Re_\theta = 2e5$ ($\bullet$), $3.5e5$ ($\blacksquare$), $5e5$ ($\blacktriangle$).

Fig. 13. Comparison between G=0.0297 at $Re_\theta = 1.5e5$ (○), 2.2e5 (□), 3e5 (◇), 3.3e5 (△), vs. Yuan et al. [8] at $G = 0.05$ and Re_θ=1.4e5 (●), 2.1e5 (■), 2.9e5 (♦), 3.3e5 (▲).

gested that the reason for this is the lack of central air admission in Yuan et al.'s experiment meaning that all rotor pumped airflow must result from inflowing cold air at the stator, whereas in our experiment the rotor pumped airflow is a combination of centrally admitted air, and air ingested at the stator.

Finally, the average stator heat transfer result of Owen et al. [6] for $G = 0.04$, $Re_\theta = 4.8e5$ is also shown in Fig. 8. It can be seen that this is lower than our average result for the equivalent Re_θ at $G = 0.0297$. Two reasons are suggested for the discrepancy: firstly, the results of Owen et al. are averaged across the complete stator surface, rather than the outer annulus $0.6 \leqslant r/R \leqslant 1$, secondly the gap size was larger, giving average lower wall shear stress and therefore lower average wall heat transfer at the stator.

9. Conclusion

This paper has presented a novel method of measuring surface convective heat transfer in a rotor–stator system using thin film electrical heaters constructed on a printed circuit board. Heat flux is measured directly by measuring electrical power into each heater. Stator temperature can also be measured directly because of the change in resistance with temperature of the copper tracks forming each heater. The method provides accurate radially resolved measurements of heat transfer from an isothermal surface.

Using the heater array, measurements have been made of stator heat transfer in a partially enclosed rotor–stator disc system. Stator heat transfer is an important factor in the design of disc type electrical machines such as axial flux permanent magnet motors and generators. As discussed in Section 3, very limited stator heat

transfer information is available that is relevant to this type of machine. The results presented here highlight the importance of peripheral fluid inflow at the stator in determining the stator heat transfer at outer radii.

References

[1] T. von Kármán, Über laminare und turbulente Reibung, Z. Angew. Math. Mech 1 (4) (1921) 233–235.
[2] L. Dorfman, Hydrodynamic Resistance and the Heat Loss of Rotating Solids, Oliver & Boyd, 1963.
[3] Engineering Sciences Data Unit, Flow in Rotating Components – Discs, Cylinders and Cavities, ESDU data Sheet 07004, IHS ESDU, 2007.
[4] J. Daily, R. Nece, Chamber dimension effects on induced flow and frictional resistance of enclosed rotating disks, ASME J. Basic Eng. 82 (1) (1960) 217–232.
[5] J. Owen, R. Rogers, Flow and heat transfer in rotating-disc systems, Rotor–Stator Systems, first ed., vol. 1, Research Studies Press, 1989.
[6] J. Owen, C. Haynes, F. Bayley, Heat transfer from an air-cooled rotating disk, Proceedings of the Royal Society of London. Series A, 336 (1607), Mathematical and Physical Sciences, 1974, pp. 453–473.
[7] R. Bunker, D. Metzger, S. Wittig, Local heat transfer in turbine disk cavities: part I, rotor and stator cooling with hub injection of coolant, ASME J. Turbomach. 114 (1992) 211.
[8] Z. Yuan, N. Saniei, X. Yan, Turbulent heat transfer on the stationary disk in a rotor–stator system, Int. J. Heat Mass Transfer 46 (12) (2003) 2207–2218.
[9] S. Scowby, R. Dobson, M. Kamper, Thermal modelling of an axial flux permanent magnet machine, Appl. Therm. Eng. 24 (2) (2004) 193–207.
[10] R. Wang, M. Kamper, R. Dobson, Development of a thermofluid model for axial field permanent-magnet machines, IEEE Trans. Energy Conver. 20 (1) (2005) 80–87.
[11] W. Rohsenow, J. Hartnett, Y. Cho, Handbook of Heat Transfer, McGraw-Hill Professional, 1998.
[12] J. Han, S. Dutta, S. Ekkad, Gas Turbine Heat Transfer and Cooling Technology, Taylor & Francis, 2000.
[13] R. Boutarfa, S. Harmand, Local convective heat transfer for laminar and turbulent flow in a rotor–stator system, Exp. Fluids 38 (2) (2005) 209–221.
[14] J. Pellé, S. Harmand, Heat transfer measurements in an opened rotor–stator system air-gap, Exp. Therm. Fluid Sci. 31 (3) (2007) 165–180.
[15] J. Pellé, S. Harmand, Heat transfer study in a discoidal system: the influence of rotation and space between disks, Int. J. Heat Mass Transfer 51 (13–14) (2008) 3298–3308.
[16] A. Cooke, P. Childs, C. Long, An investigation into the uncertainty of turbomachinery disc heat transfer obtained via inverse analysis of temperature measurements, in: Proceedings of GT2006: ASME Turbo Expo 2006.
[17] T. Kowalewski, P. Ligrani, A. Dreizler, C. Schulz, U. Fey, Y. Egami, Temperature and heat flux, in: Tropea, Yarin, Foss (Eds.), Springer Handbook of Experimental Fluid Mechanics, Springer-Verlag, 2007, pp. 487–561 (Chapter 7).
[18] T. Rule, J. Kim, Heat transfer behaviour on small horizontal heaters during pool boiling of FC-72, ASME J. Heat Transfer 121 (1999) 386.
[19] A. Chapman, Fundamentals of Heat Transfer, Macmillan, 1987.
[20] F. Incropera, D. DeWitt, T. Bergman, A. Lavine, Fundamentals of Heat and Mass Transfer, John Wiley and Sons, Inc., 2007.
[21] J. Owen, C. Haynes, Design formulae for the heat loss and frictional resistance of air cooled rotating discs, in: Improvements in Fluid Mechanics and Systems for Energy Conversion IV, Hoepli, Milan, 1976, pp. 127–160.